arXiv:cond-mat/0510789v1 [cond-mat.mes-hall] 28 Oct 2005

Local transport in a disorder-stabilized correlated insulating phase

M. Baenninger, A. Ghosh, M. Pepper, H. E. Beere, I. Farrer, P. Atkinson, D. A. Ritchie
Cavendish Laboratory, University of Cambridge, Madingley Road, Cambridge CB3 0HE, United Kingdom
(Dated: February 2, 2008)

We report the experimental realization of a correlated insulating phase in 2D GaAs/AlGaAs heterostructures at low electron densities in a limited window of background disorder. This has been achieved at mesoscopic length scales, where the insulating phase is characterized by a universal hopping transport mechanism. Transport in this regime is determined only by the average electron separation, independent of the topology of background disorder. We have discussed this observation in terms of a pinned electron solid ground state, stabilized by mutual interplay of disorder and Coulomb interaction.

PACS numbers: 73.21.-b, 73.20.Qt

In the presence of Coulomb interaction, both magnetic field and disorder are predicted to stabilize many-body charge-ordered ground states.[1,2] Strong perpendicular magnetic field $B_\perp$ quenches the vibrational motion of electrons, and has been extensively exploited to realize a charge-density wave (CDW) ground state in systems with weak background disorder.[3,4] Despite the effort however, the nature of localization in such systems has been controversial, with both pinned Wigner solid (WS) formation and inhomogeneity-driven percolation transition being suggested.[5] On the other hand, disorder stabilizes Coulomb correlation effects by introducing a pinning gap $\Delta_{\rm pin}$ in the phonon density of states, which provides a long wavelength cutoff.[2] This has led to the theoretical prediction of several forms of CDW ground states at zero or low $B_\perp$. Systematic experimental investigations on such possibilities, however, have been rare, and form the subject of this work.

Increasing the magnitude of background potential fluctuations increases $\Delta_{\rm pin}$ which stabilizes the CDW phases to higher temperatures. In modulation-doped GaAs/AlGaAs heterostructures, where disorder primarily arises from the charged dopant ions,[6] $\Delta_{\rm pin} \sim \exp\left(-4\pi\delta_{\rm sp}/\sqrt{3}r_{\rm ee}\right)$ depends strongly on the setback distance $\delta_{\rm sp}$ that separates the 2D electron system (2DES) and the dopants, where $r_{\rm ee}$ is the mean distance between the electrons in the 2DES.[7,8] However, disorder affects the ground state transport in two critical ways. First, presence of $\Delta_{\rm pin}$ disintegrates the CDW phase into domains of finite size $\lambda_{\rm d} \sim$ sound velocity$/\Delta_{\rm pin}$. At strong pinning, $\lambda_{\rm d}$ becomes microscopically small, leading to significant averaging in transport measurements with conventional macroscopic devices. Second, strong potential fluctuations can also result in a "freezing" of transport below a certain percolation threshold even when electron density ($n_{\rm s}$) is relatively high, thereby making the regime of strong effective Coulomb interaction inaccessible.

Here, we show that these difficulties can be largely overcome by using modulation-doped heterostructures of mesoscopic dimensions. In such devices transport freezes at much lower $n_{\rm s}$ in comparison to macroscopic devices at the same $\delta_{\rm sp}$ or disorder, thereby allowing transport at a large interaction parameter $r_{\rm s} = 1/a^*_{\rm B}\sqrt{\pi n_{\rm s}} \sim 7-8$ ($a^*_{\rm B}$ is the effective Bohr radius), even when $\delta_{\rm sp}$ is relatively small. Typical dimension L of our devices in the current carrying direction was chosen to be $\sim 2-4\mu$m, which is also similar in order of magnitude to the $\lambda_{\rm d}$ suggested by recent microwave absorption studies for pinned WS ground states.[4] The low-$B_\perp$ magnetotransport in these devices was found to display a striking universality in that the hopping distance in the localized regime was determined by $r_{\rm ee} = 1/\sqrt{n_{\rm s}}$, rather than the details of background disorder, indicating an unusual self-localization of electrons at sufficiently low $n_{\rm s}$.

We have used Si modulation-doped GaAs/AlGaAs heterostructures where $\delta_{\rm sp}$ was varied from 20 nm to 80 nm. At a fixed $n_{\rm s}$, the effect of $\delta_{\rm sp}$ on the strength of potential fluctuations is reflected in the mobility μ, as can be observed from Fig. 1b. Both monolayer (δ)- and bulk-doped wafers were used. Relevant properties of the devices are given in Table I. Devices were cooled from room temperature to 4.2 K over 24 - 36 hours to allow maximal correlation in the dopant layer (redistribution of DX-centers).[9] This slow cooldown technique also lead to excellent reproducibility over repeated thermal cycles. Electrical measurements were carried out with standard low frequency (7.2 Hz) four-probe technique with excitation current of $\sim 0.01-0.1$ nA to minimize heating

TABLE I: Geometrical and structural property of the devices. n_δ is the density of Si dopants, and W is the width. The background doping concentration is $\lesssim 10^{14}$cm^{-3} in all devices.

Wafer	Device	$\delta_{\rm sp}$ nm	n_δ 10^{12}cm^{-2}	$W \times L$ μm$\times\mu$m	Doping
A2407	A07a	20	2.5	8×2	δ
	A07b	20	2.5	8×3	δ
A2678	A78a	40	2.5	8×2.5	δ
	A78b	40	2.5	8×4	δ
A2677	A77	40	$-^a$	8×3	Bulk
	A77L	40	$-^a$	100×900	Bulk
C2367	C67	60	0.7	8×3	δ
T546	T46	80	1.9	8×3	δ

[a]The doping concentration of bulk doped devices is 2×10^{18}cm^{-3} over a range of 40nm.

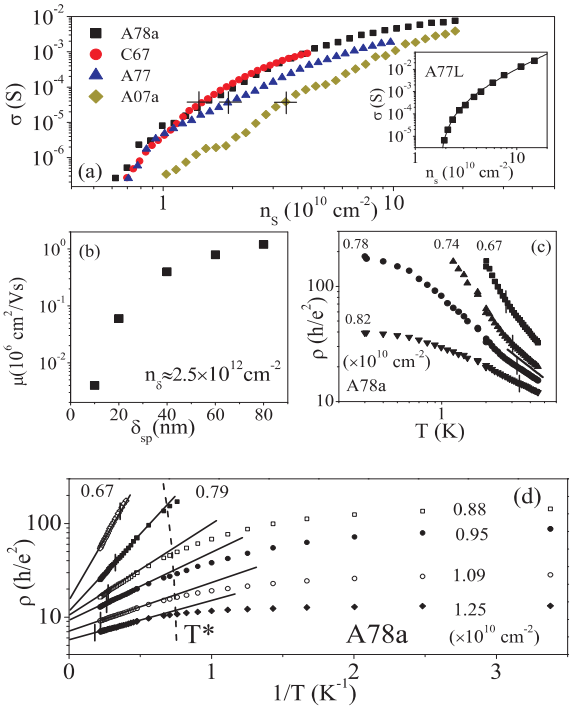

FIG. 1: (Color online) (a) Conductivity (σ) of mesoscopic samples as a function of electron density n_s at $T \approx 0.3$ K. The crosses denote n_s^* for individual samples (see text). Inset: n_s-dependence of σ for a macroscopic Hall bar A77L. The solid line is the best fit of a classical percolation-like scaling relation $\sigma \sim (n_s - n_c)^\gamma$. (b) δ_{sp} dependence of mobility at constant n_s and n_δ for heterostructures similar to those used in presented work (c) Resistivity (ρ) as a function of temperature measured at $B_\perp = 1$ T. The solid line represent a power law of $\sim T^{-1}$, vertical lines in (c) and (d) indicate the Fermi temperatures T_F. (d) Activation and saturation of ρ at $B_\perp = 1.5$ T.

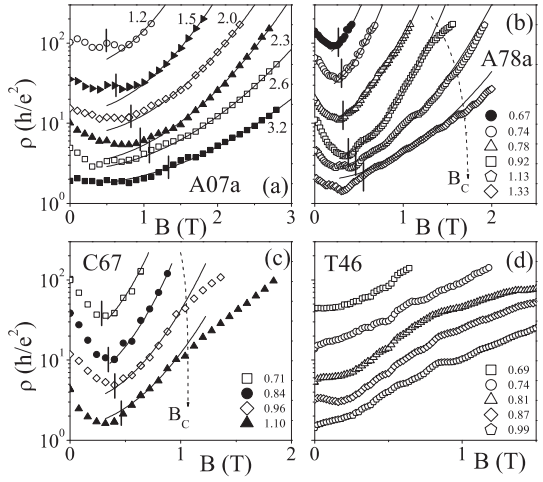

FIG. 2: Typical magnetoresistivity traces in four samples with varying level of disorder. The vertical lines denote $\nu = 1$. The numbers indicate electron density in units of 10^{10} cm^{-2}. B_c denotes the field scale up to which a quadratic $B_\perp$-dependence could be observed. The parameters α and ρ_B were obtained from the slope and y-intercept of linear fits to $\ln(\rho) - B_\perp^2$ traces, respectively.

and other nonlinear effects. A direct measurement of n_s within the microscopic region was carried out with an edge-state reflection-based technique.[10]

In Fig. 1a we compare the n_s-scale of localization transition at $B_\perp = 0$ and $T = 0.3$ K in macroscopic and microscopic devices from the same wafer. In a standard 100μm$\times 900\mu$m Hall bar, as illustrated with wafer A2677, the linear conductivity $\sigma \to 0$ (A77L: Inset of Fig. 1a) at ~ 3 times the n_s compared to the mesoscopic sample (A77) from the same wafer. Further, σ in the large sample A77L shows excellent classical percolation-like scaling $\sigma \sim (n_s - n_c)^\gamma$ ($n_c = 1.72 \times 10^{10}$ cm^{-2}), where $\gamma \approx 2$, implying a inhomogeneity-driven percolation transition at nonzero T[5] (solid line in inset of Fig. 1a). Similar scaling in the mesoscopic systems, however, was found to be difficult, with unphysically large estimates of $\gamma \sim 3.2 - 3.7$ (not shown), indicating a different mechanism of localization transition.

As n_s is lowered below a sample-dependent characteristic scale n_s^* (denoted by the crosses in Fig. 1a), onset of strong localization is identified by the resistivity ρ ($= 1/\sigma$) exceeding $\approx h/e^2$. At $n_s \ll n_s^*$, the T-dependence of ρ at a fixed n_s can be divided into three regimes, as illustrated with A78a: First, transport in the classical regime at $T \gtrsim T_F$ is magnified in Fig. 1c, where T_F is the Fermi temperature. In this regime $\rho \propto T^{-\beta}$, where $\beta \sim 1$ (indicated by the solid line). As T is decreased, the onset of the quantum regime ($T \lesssim T_F$) results in stronger increase in ρ with decreasing T. Note that the clear classical to quantum crossover implies a well-defined T_F, and hence a uniform charge density distribution down to the lowest $n_s \sim 6.5 \times 10^9$ cm^{-2} (In A77L, inhomogeneity sets in at n_s as large as $\sim 4 - 5 \times 10^{10}$ cm^{-2}). In the quantum regime and for $T_F > T > T^*$, Fig. 1d shows that the behavior of ρ is activated with $\rho(T) = \rho_3 \exp(\epsilon_3/k_B T)$, where ϵ_3 is the activation energy. From the n_s- and $B_\perp$-dependence of the pre-exponential ρ_3, we have shown earlier that the transport mechanism in this regime corresponds to nearest-neighbor hopping.[10] Below the characteristic scale $T^* \sim 1$ K, variation of ρ becomes weak, tending to a finite magnitude even in the strongly localized regime. This saturation in the insulating regime cannot be explained in terms of an elevated electron temperature due to insufficient thermal coupling to the lattice since T^* depends only weakly on electron density up to $n_s \sim n_s^*$ (Fig. 1d), and the damping of Shubnikov-de Haas oscillations in the metallic regime shows the base electron temperature to be ≈ 300 mK.

In order to explore the physical mechanism behind the weak T-dependence of ρ, we have carried out extensive magnetoresistivity (MR) measurements at the base T. Figs. 2a to 2d show the $B_\perp$-dependence of MR in the insulating regime of four devices with increasing δ_{sp} from 20 nm to 80 nm. In general, we find a strong negative MR in A07, A78 and C67 at low $B_\perp$, which can be attributed

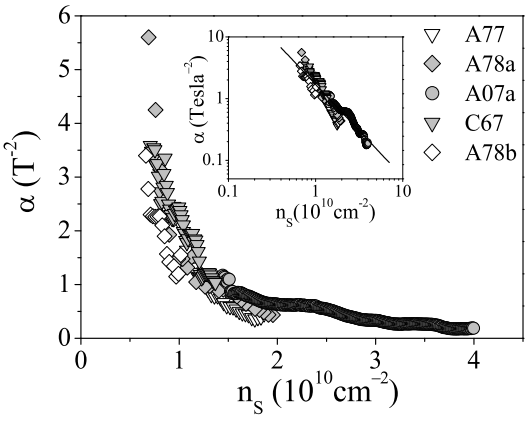

FIG. 3: Absolute magnitude of α obtained from the slope of $\ln(\rho) - B_\perp^2$ traces for five different samples. Inset shows the same data in a log-log scale. The slope of the solid line is $-3/2$.

to interference of hopping paths. The negative MR is followed by an exponential rise in ρ as $B_\perp$ is increased further. We have recently shown that the logarithm of such a positive MR at low $B_\perp$ varies in a quadratic manner with $B_\perp$, i.e., $\rho(B_\perp) = \rho_B \exp(\alpha B_\perp^2)$, where ρ_B and α are n_s-dependent factors.[10] Such a variation, denoted by the solid lines in Fig. 2, is found to be limited to $n_s \lesssim n_s^*$, and extends over a $B_\perp$-scale of B_c, where B_c was found to decrease rapidly as δ_{sp} is increased. Note that in T46 (lowest disorder), neither a clear negative MR nor an exponential $B_\perp^2$-dependence were observed. A physical significance of B_c and of the qualitatively different MR behavior of T46 will be discussed later.

The observed behavior of ρ can be naturally explained in the framework of tunnelling of electrons between two trap sites separated by a distance r_{ij}. In weak $B_\perp$, such that the magnetic length $\lambda = \sqrt{\hbar/eB_\perp} \gg \xi$, where ξ is the localization length, the asymptotic form of the hydrogenic wave function changes from $\psi(r) \sim \exp(-r/\xi)$ to $\psi(r) \sim \exp(-r/\xi - r^3\xi/24\lambda^4)$.[11] This leads to a MR, $\rho(B_\perp) = \rho_0 \exp(2r_{ij}/\xi) \exp(Ce^2 r_{ij}^3 \xi B_\perp^2/12\hbar^2)$, which implies

$$\rho_B = \rho_0 \exp(2r_{ij}/\xi) \quad \text{and} \quad \alpha = Ce^2 r_{ij}^3 \xi/12\hbar^2. \qquad (1)$$

While ρ_B depends on the tunnelling probability at $B_\perp = 0$, α denotes the rate of change of this probability when $B_\perp$ is switched on. Importantly, both parameters provide information on the intersite distance r_{ij}, as well as ξ independently. The parameter $C \sim 0.5 - 1$ depends on the number of bonds at percolation threshold in the random resistor network (we shall subsequently assume $C \approx 1$). Since conventional hopping sites are essentially impurity states, both α and ρ_B are expected to be strongly disorder dependent. Note that, since wave function overlap plays a critical role in transport, a direct source-to-drain tunnelling is ruled out in our case.[12]

From the MR data we have evaluated α and ρ_B from the slope and intercept of the $\ln(\rho) - B_\perp^2$ traces. Further details of the analysis can be found elsewhere.[10] In Fig. 3 we have shown α as a function of n_s for five different samples up to the corresponding n_s^*. Strikingly, the absolute magnitudes of α from different samples are strongly correlated, and can be described by an universal n_s-dependent function over nearly two orders of magnitude. At stronger disorder (e.g., A07), localization occurs at a higher n_s resulting in a lower α, while at lower disorder (e.g. C67) localization occurs at lower n_s yielding a larger magnitude of α. This indicates that magnetotransport in such mesoscopic samples is not determined directly by disorder, but by n_s in the localized regime. Qualitatively, the decreasing behavior of α with increasing n_s itself is inconsistent with the single-particle localization in an Anderson insulator.[10,13]

From the strong sample-to-sample correlation in the magnitude of α, a disorder-associated origin of r_{ij}, is clearly unlikely. For example, taking $r_{ij} \sim \delta_{sp}$ will lead to distinct sets of α for wafers with different δ_{sp}. However, in the context of a pinned CDW ground state, another relevant length scale is r_{ee}. Indeed, in case of tunnelling events over a mean electron separation, i.e., $r_{ij} \approx r_{ee}$, we find that Eq. 1 describes both absolute magnitude, as well as the n_s-dependence of α quantitatively. Using $r_{ij} \approx 1/\sqrt{n_s}$, Eq. 1 leads to $\alpha \propto n_s^{-3/2}$, as indeed observed experimentally (solid line in the inset of Fig. 3). Allowing for sample-to-sample variation, we find $\alpha = (1.7 \pm 0.5) \times 10^{21}/n_s^{3/2}$ T^{-2} from which, using Eq. 1, we get $\xi = 9.0 \pm 2.6$ nm, which is close to a_B^* in GaAs (≈ 10.5 nm).

The analysis can be immediately checked for consistency from the r_{ee}-dependence of ρ_B. From Fig. 4, we find that ρ_B increases strongly with increasing r_{ee} when $n_s \ll n_s^*$, as expected in the simple tunnelling framework (Eq. 1). In spite of the scatter, the overall slopes of the $\ln(\rho_B) - r_{ee}$ plots are similar in different samples (solid lines) with ξ estimated to be $\approx 13 \pm 4$ nm, agreeing with that obtained from the analysis of α. Note that the ρ_B deviates from the exponential dependence, and tends to saturate as $n_s \to n_s^*$. While this is not completely understood at present, we note that the saturation in ρ_B occurs within the range $\rho_B \sim 1 - 2 \times h/e^2$, irrespective of sample details. Similar universality in the hopping pre-exponential has been observed in the context of T-dependence of ρ in variable-range hopping,[14] and has been suggested to indicate an electron-electron interaction mediated energy-transfer mechanism.

We now discuss the physical scenario which could lead to the electron separation-dependent hopping transport. We show that our observations can be explained in the theoretical framework of defect motion in a quantum solid that was originally developed by Andreev and Lifshitz in context of solid He^3,[15] and later adapted for a WS ground state.[16,17] In our case, transport in both quantum and classical regime can be understood in terms of tunnelling of localized defects in an interaction-induced

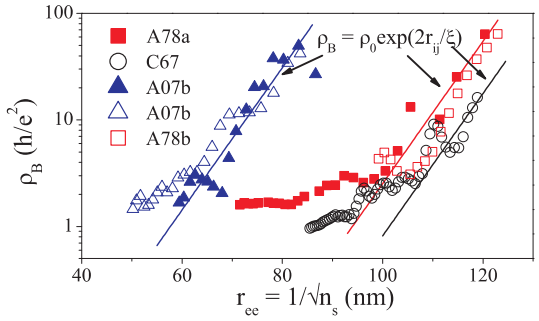

FIG. 4: (Color online) The dependence of ρ_B on the average electron separation r_{ee} in five different samples. The slope of the solid lines gives an estimate of ξ (Eq. 1).

pinned electron solid phase as n_s is reduced below the melting point n_s^*. The defects, which act as quasiparticles at low T, can arise from regular interstitials, vacancies, dislocation loops etc., as well as from zero-point vibration of individual lattice sites.[15] The scale of zero-point fluctuation $\sim h/r_{ee}\sqrt{m^* U_C} \approx 2\pi/\sqrt{r_s} \gtrsim 1$, is indeed strong in our case over the experimental range of n_s, where $U_C \approx e^2/4\pi\epsilon r_{ee}$ is the interatomic interaction energy scale.

In the quantum regime, the transport at higher T ($T_F \gg T \gg T^*$) is predicted to be thermally activated nearest-neighbor hopping of localized defects, while at lower T ($\ll T^*$) tunnelling of such defects leads to a T-independent transport.[15] While this clearly describes the weak T-dependence of ρ at low temperatures (Fig. 1d), the strongest support to this picture comes from the fact that the natural length scale of tunnelling is indeed the average electron separation r_{ee}. This immediately explains the unusual n_s (or r_{ee})-dependence of both α and ρ_B, as well as the apparent insensitivity of these parameters to local disorder. The negative MR at low $B_\perp$ caused by destruction of interference is then expected to persist up to a $B_\perp$ corresponding to $\nu = n_s h/eB_\perp \sim 1$ (one flux quantum ϕ_0 within an area of r_{ee}^2), as indeed observed in our experiments (Fig. 2). The tunnelling of defect scenario also allows an estimate of the crossover scale $k_B T^* = \epsilon_3/\ln(\Delta_{pin}/\Delta\epsilon)$,[15] where $\Delta\epsilon$ is the bandwidth. For a pinned WS ground state, using the expression of Δ_{pin} in Ref.[8], experimentally measured ϵ_3, and $\Delta\epsilon \sim h^2/8m^* r_{ee}^2$, we find $T^* \sim O$[1 Kelvin] over the experimental range of n_s in A78a, giving good order-of-magnitude agreement to the observed scale of T^*. Finally, the behavior of $\rho \sim T^{-1}$ in the classical regime ($T > T_F$)(Fig. 1c) has also been recently observed,[18] and interpreted in terms of transport mediated by defect-type topological objects (Fermi-liquid droplets) in the WS phase.[16]

In presence of pinning, the MR-data suggests the asymptotic form of the wave function $\psi(r) \sim \exp(r/\xi)$, where $\xi \approx a_B^*$. However, the interplay of confinement arising from the magnetic potential and disorder pinning is expected to be critical in determining $\psi(r)$, with disorder pinning dominating at low $B_\perp$. This is expected to result in the upper cutoff B_c that decreases with decreasing disorder, as observed experimentally. The intricate interplay between disorder, electron-electron interaction and magnetic field is further illustrated by the absence of a clear $B_\perp^2$ dependence of the MR in T46 (largest δ_{sp}), which could be explained by a prohibitively small B_c or the very instability of the solid phase at sufficiently low disorder. On the other hand, devices with $\delta_{sp} \lesssim 10$nm showed inhomogeneity-driven Coulomb blockade oscillations in the localized regime, making the investigation of such a charge correlated state impossible. A quantitative understanding of the scale of B_c, as well as the specific spatial structure of the ground state in the intermediate disorder regime, will require further investigations, which are presently in progress.

[1] B. Tanatar and D. M. Ceperley, Phys. Rev. B **39**, 5005 (1989); A. G. Eguiluz, A. A. Maradudin and R. J. Elliott, *ibid.* **27**, 4933 (1983); A. A. Koulakov, M. M. Fogler and B. I. Shklovskii, Phys. Rev. Lett. **76**, 499 (1996).

[2] J. S. Thakur and D. Neilson, Phys. Rev. B **54**, 7674 (1996); A. A. Slutskin, V. V. Slavin, and H. A. Kovtun, *ibid.* **61**, 14184 (2000); G. Benenti, X. Waintal and J. -L. Pichard, Phys. Rev. Lett. **83**, 1826 (1999); R. Jamei, S. Kivelson and B. Spivak, *ibid.* **94**, 056805 (2005); S. T. Chui and B. Tanatar, *ibid.* **74**, 458 (1995).

[3] H. W. Jiang, R. L. Willet, H. L. Stormer, D. C. Tsui, L. N. Pfeiffer and K. W. West, Phys. Rev. Lett. **65**, 633 (1990); V. Goldman, M. Santos, M. Shayegan and J. E. Cunningham, *ibid.* **65**, 2189 (1990); H. Manoharan Y. W. Suen, M. B. Santos and M. Shayegan, *ibid.* **77**, 1813 (1996); J. Yoon, C. C. Li, D. Shahar, D. C. Tsui and M. Shayegan, *ibid.* **82**, 1744 (1999).

[4] P. D. Ye, L. W. Engel, D. C. Tsui, R. M. Lewis, L. N. Pfeiffer and K. West, Phys. Rev. Lett. **89**, 176802 (2002); Y. Chen, R. M. Lewis, L. W. Engel, D. C. Tsui, P. D. Ye, L. N. Pfeiffer and K. W. West, *ibid.* **91**, 016801 (2003).

[5] A. A. Shashkin, V. T. Dolgopolov, G. V. Kravchenko, M. Wendel, R. Schuster, J. P. Kotthaus, R. J. Haug, K. von Klitzing, K. Ploog, H. Nickel and W. Schlapp, Phys. Rev. Lett. **73**, 3141 (1994); Y. Meir, *ibid.* **83**, 3506 (1999); S. Das Sarma, M. P. Lilly, E. H. Hwang, L. N. Pfeiffer, K. W. West and J. L. Reno, *ibid.* **94**, 136401 (2005).

[6] A. L. Efros, Solid State Commun. **65**, 1281 (1988); A. L. Efros, F. G. Pikus and V. G. Burnett, Phys. Rev. B **47**, 2233 (1993).

[7] I. M. Ruzin, S. Marianer and B. I. Shklovskii, Phys. Rev. B **46**, 3999 (1992).

[8] S. T. Chui, J. Phys.: Condens. Matter **5**, L405 (1993).

[9] E. Buks, M. Heiblum and H. Shtrikman, Phys. Rev. B **49**, 14790 (1994); M. Stopa, *ibid.* **53**, 9595 (1996).

[10] A. Ghosh, M. Pepper, H. E. Beere and D. A. Ritchie, Phys.

Rev. B **70**, 233309 (2004).
[11] B. I. Shklovskii, Fiz. Tekh. Poluprovodn. **17** 2055 (1983) [Sov. Phys. Semicond. **17**, 1311 (1983)]; B. I. Shklovskii and A. L. Efros, in *Electronic Properties of Doped Semiconductors*, Vol. 45 of Springer Series in Solid-State Sciences (Springer, Berlin, 1984).
[12] A. K. Savchenko, V. V. Kuznetsov, A. Woolfe, D. R. Mace, M. Pepper, D. A. Ritchie and G. A. C. Jones, Phys. Rev. B **52**, R17021 (1995).
[13] G. Timp and A. B. Fowler, Phys. Rev. B **33**, 4392 (1986).
[14] S. I. Khondaker, I. S. Shlimak, J. T. Nicholls, M. Pepper and D. A. Ritchie , Phys. Rev. B **59**, 4580 (1999); W. Mason, S. V. Kravchenko, G. E. Bowker and J. E. Furneaux, *ibid.* **52**, 7857 (1995).
[15] A. F. Andreev and I. M. Lifshitz, Zh. Eksp. Teor. Fiz. **56**, 2057 (1969) [Sov. Phys. JETP **29**, 1107 (1969)].
[16] B. Spivak, Phys. Rev B **67**, 125205 (2003).
[17] G. Katomeris, F. Selva and J. -L. Pichard, Eur. Phys. J. B **31**, 401 (2003), *ibid.* **33**, 87 (2003).
[18] H. Noh, M. P. Lilly, D. C. Tsui, J. A. Simmons, L. N. Pfeiffer and K. W. West, Phys. Rev. B **68**, 241308(R) (2003).